Iranian Journal of Catalysis 10(3), 2020, 235-245

IRANIAN JOURNAL OF CATALYSIS

Photocatalytic degradation of malachite green dye using $NiAl_2O_4$ and Co doped $NiAl_2O_4$ nanophotocatalysts prepared by simple one pot wet chemical synthetic route

M. Arunkumar, A. Samson Nesaraj*

Department of Applied Chemistry, Karunya Institute of Technology and Sciences (Deemed to be University), Karunya Nagar, Coimbatore - 641114, India.

Received 8 March 2020; received in revised form 7 August 2020; accepted 31 August 2020

ABSTRACT

Novel metal oxides have been studied worldwide due to their potential uses in ecological refinement, particularly to eliminate organic impurities present in water. In this work, we report the preparation of $Ni_{1-x}Co_xAl_2O_{4-\delta}$ (where x=0, 0.05, 0.10, 0.15 and 0.20) nanoparticles by simple chemical precipitation route. The as-synthesized spinel particles were characterized by X-ray diffraction (XRD), Fourier transform infrared spectroscopy (FT-IR), particle size analysis, scanning electron microscopy (SEM) and energy dispersive X-ray analysis (EDX), UV-Vis Spectroscopy (UV) and Photo Luminescence (PL) Spectroscopy techniques. The XRD results affirmed the development of the cubic structure in all the samples. FT-IR confirmed the presence of the M-O bond. Particle characteristics statistics showed the existence of particles in the range of 36-741 nm range. SEM analysis strengthened the presence of various sized grains (nano and micron) in the samples. EDX analysis affirmed the existence of an appropriate amount of elements (Ni, Al, Co and O) in all the samples. The band gap of Co doped $NiAl_2O_4$ was in between 2.8 – 3.0 eV, which was in line with the reported data. The PL spectra exhibited a strong peak at around 450 nm in the samples. From UV studies, the λ_{max} was around 310 nm in all the prepared samples. The photoluminescent characteristics of the samples were confirmed by PL studies and their photoemission was found at 437 nm. Among the samples studied, the parent $NiAl_2O_4$ shows more efficiency in degrading the malachite green (MG) dye than other Co doped $NiAl_2O_4$ photocatalysts under the irradiation of visible light at the wavelength of 616nm at normal temperature.

Keywords*: Co doped $NiAl_2O_4$ nanoparticles, Organic pollutant, Photodegradation, Characterization, Photocatalysis.*

1. Introduction

Water contamination is one of the overall issues these days and this can legitimately influence the strength of living life forms. As a result of the enormous increase of industries, sewages from the majority of the ventures are released straightforwardly or by implication into the streams of water without eliminating the destructive or hazardous substances and this may contaminate water. There are various assortments of aqueous toxins accessible, which incorporate waste synthetic substances, squander natural matter, nearness of destructive pathogens, and so on. Water contamination is a consuming worldwide issue; consequently, the advancement of reasonable eco-accommodating treatment techniques is more necessary at present [1].

*Corresponding author.
Email: drsamson@karunya.edu (A. Samson Nesaraj)

Researchers have built up certain strategies for the purification of contaminated water, such as the addition of adsorbents, electrolyte decomposition, ion exchange method, biological methods and so on. These purification techniques are never an option at enormous level because of significant expense and therefore, some other strategies are required, which are dependable also as green concoction in nature. Photocatalysis gives the green passage to degradation of numerous organic impurities. So photocatalysis is recognized as an assuring innovation for the purification of impure water [2]. Conservatively, semiconductors act as a catalyst in the photocatalytic degradation of dyes. Also, TiO_2, metal doped TiO_2, metal oxides and metal composites are widely responsible for the elimination of dyes in contaminated water [3]. Mehrabadi and Faghihian [4] have eliminated the herbicide, namely 2, 4-dichlorophenoxy acetic acid by the photocatalyst

zeolite clinoptilolite with TiO_2 under UV light irradiation. However, one disadvantage of TiO_2 is that it exhibits high band gap energy of 3.2 eV; therefore, passing of UV light is mandatory to activate TiO_2. Also, TiO_2 without agents like Pt or RuO_2, the combination of charge carrying ions happens in nanoseconds, therefore the photocatalytic degradation is found to be low [5]. Abedi et.al [6] have explored a novel 3D metallic-organic framework (MOF) based photocatalyst and its application in the elimination of bromocresol green dye in water in the presence of visible light irradiation. Mehrabadi and Faghihian [7] have tried doping TiO_2 on clinoptilolite nanoparticles and studied its photocatalytic activity on the removal of organic compound mixture of 2,4-dichlorophenoxyacetic acid (2,4-D), and 2-methyl-4-chlorophenoxyacetic acid(MCPA) in the presence of UV and sunlight. Derikvandi and Nezamzadeh-Ejhieh [8] have used SnS_2–ZnS on clinoptilolite nanoparticles for the photocatalytic elimination of an oil containing water solution comprising phenol as the main constituent. Ghattavi and Nezamzadeh-Ejhieh [9] have developed a AgBr-g-C_3N_4 nanocomposite which shows substantial improvement in the photocatalytic degradation of methyl orange (MO) in the irradiation of visible light. Jafari and Nezamzadeh-Ejhieh [10] have synthesized novel photocatalyst by dispersing AgX (X = I, Br, Cl) in nanosized clinoptilolite particles (NCP). The acquired nanocomposites (AgX-NCP) were useful in the degradation of the mixture containing 4-methoxy aniline and 4-chloro-3-nitroaniline by mercury lamp irradiation. Khatri et al. [11] have reviewed the advancement in coloring cotton materials with sensitive dyes for lessening contamination.

Buthiyappan et al. [12] have reviewed the elimination of numerous fabric dyes by a variety of photocatalysts and adsorbents. Further, they have reviewed the drawbacks of normal advanced oxidation processes (AOPs) for textile use and recommended elucidations to eliminate defects. Benkhaya et al. [13] have reviewed the categories, modern production and uses of fabric colorants. Azari et al. [14] have reviewed the meta-analysis of pigments adsorption using carbon centered sources. Katheresan et al. [15] have reviewed the efficacy of several new techniques to eliminate contaminants from water.

Nezamzadeh-Ejhieh et al. [16] have incorporated CuO on clinoptilolite nanoparticles using the ion-exchange method followed by calcination. The acquired nanocomposite (CuO-NCP) was good in photodecolorizing the blend of Methylene Blue and Bromophenol Blue. The degradation efficiency of 61% and 32% were reported for MB and BPB under 3 hours of irradiation. Nezamzadeh-Ejhieh et. al [17] have reported a photodegradation of crystal violet using CdS nanoparticles incorporated on zeolite A. They have reported about 80% of photodecolorization in about 20 min.

Nano-crystalline aluminates having the molecular formula MAl_2O_4 (M= Ni, Zn, Mn, Co, Mg, Sr, Ca and La etc.) fascinate more researchers because of their flexible, functional applications. Aluminates were preferred mostly because they are thermally strong, good mechanical behavior, hydrophobic activity, and less surface acidity. Nickel aluminates, highly significant spinel, attracting many scientists due to their magnetic behavior, catalytic properties, coloring agents and refractory materials [18]. The catalytic properties of $NiAl_2O_4$ are due to its larger surface area. Generally, materials with a larger surface area will have a smaller particle size. Thus, the preparation of $NiAl_2O_4$ nanoparticles is of great significance [19]. Since the band gap of this material is large (3.0 eV), it is not easy to convert into visibly active material. To enhance this property, metals such as Zn, Mn, Co, Ce, Ba, etc. can be doped in TiO_2. In general, co-doping is used to increase the solubility of the dopant, which can further enhance the activation rate of an oxide photocatalyst by reducing the ionization energy of acceptors and donors, and increasing the carrier mobility [20, 21].

A few methods to synthesis $NiAl_2O_4$ nanoparticles, such as chemical solution deposition [22,23], sonochemical synthesis [24], microwave-assisted method [25,26] and polymer solution technique [27]. To prepare highly purified and nano sized materials, chemical precipitation technique is used at large [28-30]. Malachite green (MG), a member from a cationic triphenylmethane family, has found a variety of applications as coloring pigment in different enterprises, including textiles (for example, silk and fleece), food, paper, and leather. It has too been utilized for the generation of ceramics, guard against bacterial diseases, and treating scratches on fish bodies in the farming industry. Even so, it has been accounted for that this dye is profoundly harmful, mutagenic and cancer-causing. Consequently, wiping out such a toxic dye before being released into the water body is of great significance [31, 32]. The photocatalytic efficiency of the Cu-substitution of $NiAl_2O_4$ is already done on the degradation of congo red (CR) dye using the irradiation of sunlight. The efficient catalyst is $Ni_{0.2}Cu_{0.8}Al_2O_4$ with a removal conversion of 90.55% of the dye after 180 min. [33]. The photocatalytic activity of $NiAl_2O_4$, $CuAl_2O_4$ and $ZnAl_2O_4$ nanoparticles were studied recently by the disintegration of four sorts of contaminants: phenol rhodamine B, heteropolyaromatic methylene blue, azoic

methyl orange, and methyl red using UV irradiation. The maximum photocatalytic efficiency is attained by removing all the organic colorants by aluminate nanoparticles in less than 100 min. [34]. No clear reports are available in studying the photocatalytic behavior of other dyes by Co doped $NiAl_2O_4$ photocatalyst materials.

In this research article, the first part has been focused on the synthesis of $NiAl_2O_4$ and cobalt doped $NiAl_2O_4$ nanoparticles by simple wet chemical synthesis route and the regular characterization to examine their structural, morphological, elements analysis and optical properties. The second part revolves around the photocatalytic behavior of $NiAl_2O_4$ and Co doped $NiAl_2O_4$ to remove the malachite green dye in water in the presence of Visible irradiation. These results are well discussed and presented in this study.

2. Experimental

2.1. Materials

Nickel nitrate (98%, Merck, India), cobalt nitrate (98%, Merck, India), sodium hydroxide (97%, Merck, India), ethanol (99.9%, CS, China) and malachite green (90%, Isochem, India) were the chemicals used in this study. All these chemicals were utilized as procured. We used double distilled water for all these reactions.

2.2. Preparation of $NiAl_2O_4$ and Co doped $NiAl_2O_4$ nanoparticles

The $NiAl_2O_4$ and Co doped $NiAl_2O_4$ spinels were synthesized by a simple wet chemical synthesis route. The aqueous solutions of nickel nitrate, cobalt nitrate and sodium hydroxide were made with the required molar concentration. These solutions were added together uniformly and agitated well for 1 hour in a magnetic stirrer at normal temperature. The attained green colored mass (precipitate) was filtered using vacuum filtration. The filtered precipitate was washed with a 5% alcohol-water mixture many times to eliminate any impurities if formed. After careful washing, the precipitate was placed in a hot air oven maintained at 60 ℃ for 2 hours. Then, the dried particles were calcined at 150, 300, 450 and 600 ℃ for 2 hours each to prepare cobalt doped nickel aluminate nanoparticles. The amount of precursor salts used for the synthesis of $NiAl_2O_4$ and Co doped $NiAl_2O_4$ nanoparticles is shown in Table 1. The flowchart for this reaction is given in Fig. 1. The main reaction for the preparation of $NiAl_2O_4$ and Co doped $NiAl_2O_4$ is shown in Eq. 1:

$$2Al(NO_3)_3 + x\ Co(NO_3)_2 + (1\text{-}x)\ Ni(NO_3)_2 + 8NaOH \rightarrow Ni_{1-x}Co_xAl_2O_{4-\delta} + 8NaNO_3 + 4H_2O \quad \textbf{(1)}$$

(where x = 0, 0.05, 0.10, 0.15 and 0.20)

2.3. Characterization

The crystallographic properties of $NiAl_2O_4$ and Co doped $NiAl_2O_4$ nanoparticles were studied by powder X-ray diffractometer (Shimadzu XRD6000). The IR transmittance spectra of $NiAl_2O_4$ and Co doped $NiAl_2O_4$ spinels were measured using Fourier Transform Infra-Red Spectrometer (Shimadzu IR Prestige 21) and KBr pellet method is used in the range from 4000-400 cm^{-1}. The particle size of the nanoparticles was estimated using Malvern Particle Size Analyzer with triple distilled water as medium. The morphology and the element ratio of $NiAl_2O_4$ and Co doped $NiAl_2O_4$ nanoparticles were studied by scanning electron microscope (SEM JEOL JSM-6610) fitted with an energy dispersive X-ray (EDX) spectrophotometer. UV spectra of the photocatalysts were analyzed by UV–Visible spectrophotometer (Shimadzu 1800) between 200 to 600nm. The PL (photoluminescence) spectra of the samples were studied using a spectrofluorometer (JASCO) at normal temperature.

2.4. Photocatalytic experiments

The photocatalytic activities of $NiAl_2O_4$ and Co doped $NiAl_2O_4$ nanoparticles were examined in a solution of malachite green (MG) dye as given below: The 50 ml of malachite green (0.2 g/L) dye solution was taken in a simple photocatalytic set up fitted with 6 W visible light source at normal temperature as shown Fig. 2.

Table 1. Amount of precursor salts used for the synthesis of $NiAl_2O_4$ and Co doped $NiAl_2O_4$ nanoparticles [volume of each solution is 100 ml].

Sample	Wt. of $Ni(NO_3)_2$ (g)	Wt. of $Co(NO_3)_2$ (g)	Wt. of $Al(NO_3)_3$ (g)	Wt. of NaOH (g)
$NiAl_2O_4$	2.91	-	7.5	3.2
$Ni_{0.95}Co_{0.05}Al_2O_{4-\delta}$	2.75	0.145	7.5	3.2
$Ni_{0.90}Co_{0.10}Al_2O_{4-\delta}$	2.61	0.291	7.5	3.2
$Ni_{0.85}Co_{0.15}Al_2O_{4-\delta}$	2.46	0.436	7.5	3.2
$Ni_{0.8}Co_{0.2}Al_2O_{4-\delta}$	2.32	0.582	7.5	3.2

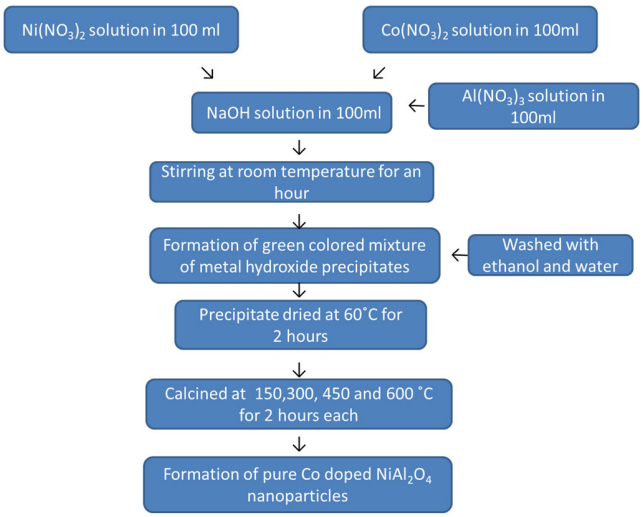

Fig. 1. Flow chart to prepare Co doped $NiAl_2O_4$ nanoparticles by chemical precipitation technique.

Fig. 2. Photocatalytic setup with Visible light.

To the dye solution, 5 mg of $NiAl_2O_4$ based catalyst were put into the solution separately and the solution was permitted to reach the equilibrium condition for about 60 minutes. At various time interims, 2 mL of the solution was taken from the set up and the UV–visible spectra were taken at 617 nm as specified in the literature [35]. The photodegradation efficiency of dye, η [36], was estimated by the Eq. 2:

$$\eta = (C_0\text{-}C_t/C_0) \times 100 \quad \textbf{(2)}$$

where 'C_0' is the initial concentration of MG solution and 'C_t' is the concentration at time t, respectively.

3. Results and Discussion

3.1. Powder X-Ray diffraction (XRD) studies

Fig. 3 illustrates the XRD display of $NiAl_2O_4$ and Co doped $NiAl_2O_4$ nanoparticles. It reveals that the peaks are well-matched with the reference JCPDS number 10-0339. The peaks found at 2θ values of 19.069, 37.008, 44.994, 59.659 and 65.532 correspond to the (111), (311), (400), (511) and (440) surface of $NiAl_2O_4$ crystal, respectively, which can be easily ascribed to a face-centered cubic (F.C.C.) phase. Additional information discloses that all the spinels had intense peaks, which indicate a good crystalline property of the sample. The crystallite size of these samples was calculated using the Scherrer formula [37] (Eq. 3):

$$D = 0.9\lambda/ \beta \cos\theta \quad \textbf{(3)}$$

where, 'D' is the average crystalline size (A˚), 'λ' is the X-ray wavelength (0.154 nm), 'θ' is the angle of diffraction and, 'β' is the full width at half maximum of the peaks. The calculated crystallite size values of all the samples are indicated in Table 2.

The theoretical [38] density (Dx) values of the samples were derived by the given formula (Eq. 4):

$$D_x\ (g/cm^3) = (Z \times M)\ /(N \times a^3) \quad \textbf{(4)}$$

where, 'Z' is the number of species in the unit cell, 'M' is the molecular weight of the sample (g/mol), 'N' is the Avogadro's number (6.023×10^{23}) and 'a' is the lattice constant (cm). The theoretical density and other factors acquired on $NiAl_2O_4$ and Co doped $NiAl_2O_4$ nanoparticles are demonstrated in Table 2. The calculated unit cell parameter of these samples is in good agreement with the published data (a = 8.083 Å) [18].

3.2. FT-IR studies

Fig. 4 indicates the FTIR spectrum of $NiAl_2O_4$ and Co doped $NiAl_2O_4$ nanoparticles.

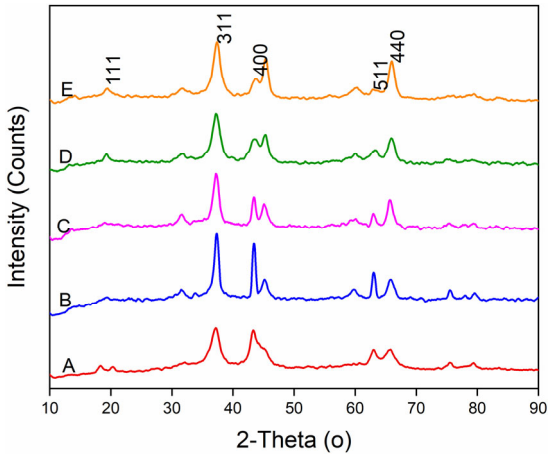

Fig. 3. XRD pattern obtained on $NiAl_2O_4$ based nanoparticles: A) Parent $NiAl_2O_4$, B) $Ni_{0.95}Co_{0.05}Al_2O_{4-\delta}$, C) $Ni_{0.90}Co_{0.10}Al_2O_{4-\delta}$, D) $Ni_{0.85}Co_{0.15}Al_2O_{4-\delta}$, E) $Ni_{0.80}Co_{0.20}Al_2O_{4-\delta}$.

Table 2. Crystallographic parameters were obtained on $NiAl_2O_4$ and Co doped $NiAl_2O_4$ nanoparticles.

Sample	Crystal structure	Unit cell parameter (Å)	Unit cell volume (Å^3)	Crystallite size (nm)	Theoretical density (g cm^{-3})
$NiAl_2O_4$	Cubic (F.C)	8.046	521.04	3.10	4.503
$Ni_{0.95}Co_{0.05}Al_2O_{4-\delta}$	Cubic (F.C)	8.022	516.26	6.50	4.545
$Ni_{0.90}Co_{0.10}Al_2O_{4-\delta}$	Cubic (F.C)	8.047	521.18	5.74	4.502
$Ni_{0.85}Co_{0.15}Al_2O_{4-\delta}$	Cubic (F.C)	8.082	527.95	12.48	4.445
$Ni_{0.80}Co_{0.20}Al_2O_{4-\delta}$	Cubic (F.C)	8.034	518.68	7.40	4.525

From Fig. 4, the band located around 3400 cm^{-1} can be assigned to the O-H stretching vibration of water, and the band near 1650 cm^{-1} assigned to the bending vibration of H-O-H [39]. Bands at 734 cm^{-1} and 540 cm^{-1} are the significant bands that can be connected to bonds of the tetrahedral and octahedral sites of the spinel [40]. The emergence of a new peak at 1540 cm^{-1} and 973 cm^{-1} shows the existence of Co doping. Overall, the spectrum of parent $NiAl_2O_4$ and other Co doped $NiAl_2O_4$ samples differ in the figure of the transmittance spectrum, indicating obvious small changes in the structure because of different dopant (Co) level concentration.

3.3. Particle size analysis

The particle size analysis curves of $NiAl_2O_4$ and Co doped $NiAl_2O_4$ nanoparticles are indicated in Fig. 5. For each of these experiments, the material is mixed with distilled water and kept in an ultrasonic bath. After 10 minutes, the sample is taken from the bath and analyzed. The data acquired from the particle size analysis on $NiAl_2O_4$ and Co doped $NiAl_2O_4$ nanoparticles is shown in Table 3.

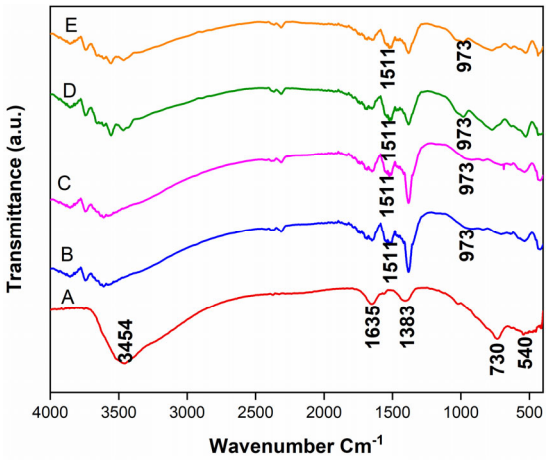

Fig. 4. FTIR transmittance spectrum on $NiAl_2O_4$ based nanoparticles: A) Parent $NiAl_2O_4$, B) $Ni_{0.95}Co_{0.05}Al_2O_{4-\delta}$, C) $Ni_{0.90}Co_{0.10}Al_2O_{4-\delta}$, D) $Ni_{0.85}Co_{0.15}Al_2O_{4-\delta}$, E) $Ni_{0.80}Co_{0.20}Al_2O_{4-\delta}$.

The results revealed that the average particle size varies between 36-741 nm range. A high-temperature calcination method may be responsible for the presence of a higher range of particles [41].

3.4. Scanning electron microscopy (SEM) studies

These SEM photographs obtained on $NiAl_2O_4$ and Co doped $NiAl_2O_4$ nanoparticles are indicated in Fig. 6. The SEM micrographs indicate the formation of nanoparticles in the samples. In all the samples, almost the grains were present together. Further, the surface morphology of samples comprises of little grains which are agglomerated and joined with each other. There may be two reasons for this formation of agglomerates (~ few µm). First, the small particles (in nanoscale) are energetically more stable in the agglomeration configuration. Second, the agglomeration of the small particles allows for crystal growth [42]. $Ni_{0.85}Co_{0.15}Al_2O_{4-\delta}$ resulted in a needle-like structure (Fig. 6D). The grains present in all the samples are found to be in the range of about 30 – 60 nm.

3.5. EDX analysis

Fig. 7 shows the EDX spectrum of $NiAl_2O_4$ and Co doped $NiAl_2O_4$ nanoparticles. The elemental analysis obtained on $NiAl_2O_4$ and Co doped $NiAl_2O_4$ is presented in Table 4. The existence of elements such as Ni, Al, Co and O in the samples is bolstered by EDX studies. The Co atomic weight percentage increases with an increase in Co doping concentration. EDX results reveal that the correct amounts of Ni, Al, Co, and O existing in the samples. Slight variation in the dopant level in the final product may be due to experimental conditions.

3.6. Studies on optical properties

The optical property of $NiAl_2O_4$ and Co doped $NiAl_2O_4$ nanoparticles was studied using UV visible technique. Fig. 8 shows that the UV absorption region of $NiAl_2O_4$ and Co doped $NiAl_2O_4$ nanoparticles in the range between 200 to 500nm. As seen from the graph, $NiAl_2O_4$ and Co doped $NiAl_2O_4$ nanoparticles exhibit a broad peak between 270 to 320 nm, with the maximum

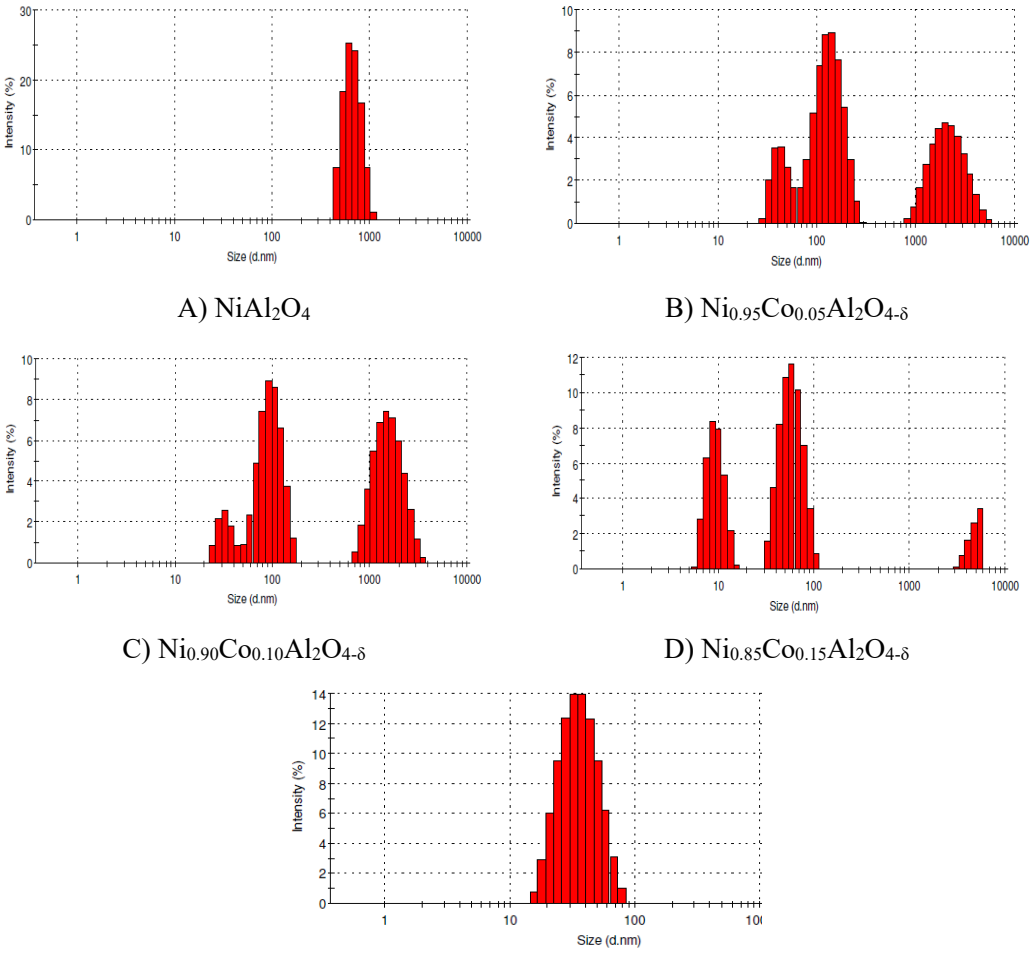

Fig. 5. Particle size distribution curves obtained on $NiAl_2O_4$ based nanoparticles A) Parent $NiAl_2O_4$, B) $Ni_{0.95}Co_{0.05}Al_2O_{4-\delta}$, C) $Ni_{0.90}Co_{0.10}Al_2O_{4-\delta}$, D) $Ni_{0.85}Co_{0.15}Al_2O_{4-\delta}$, E) $Ni_{0.80}Co_{0.20}Al_2O_{4-\delta}$.

Table 3. Particle size data obtained on $NiAl_2O_4$ and Co doped $NiAl_2O_4$ nanoparticles.

Sample	Average particle size (nm)
$NiAl_2O_4$	741
$Ni_{0.95}Co_{0.05}Al_2O_{4-\delta}$	148
$Ni_{0.90}Co_{0.10}Al_2O_{4-\delta}$	146
$Ni_{0.85}Co_{0.15}Al_2O_{4-\delta}$	26
$Ni_{0.80}Co_{0.20}Al_2O_{4-\delta}$	36

value at 310nm approximately. To find out the direct band gap for $NiAl_2O_4$ and Co doped $NiAl_2O_4$ nanoparticles, Tauc [43] plot used is indicated in Eq. 5.

$$\alpha h\nu = A(h\nu - E_g)^n \quad \textbf{(5)}$$

where, 'α' is the absorption coefficient, 'A' is a constant and n = ½ (for direct band gap). The drawn plot of $(\alpha h\nu)^2$ versus $h\nu$ provides the linear line at a certain point. The extrapolating the straight line gives the optical band gap (Eg) value, as shown in Fig. 9. The obtained band gap values were 3.088, 3.03, 2.952, 2.857 and 2.804 eV respectively for $NiAl_2O_4$, $Ni_{0.95}Co_{0.05}Al_2O_{4-\delta}$, $Ni_{0.90}Co_{0.10}Al_2O_{4-\delta}$, $Ni_{0.85}Co_{0.15}Al_2O_{4-\delta}$ and $Ni_{0.80}Co_{0.20}Al_2O_{4-\delta}$ nanoparticles, which is in good agreement with the stated value of 2.9 eV [44].

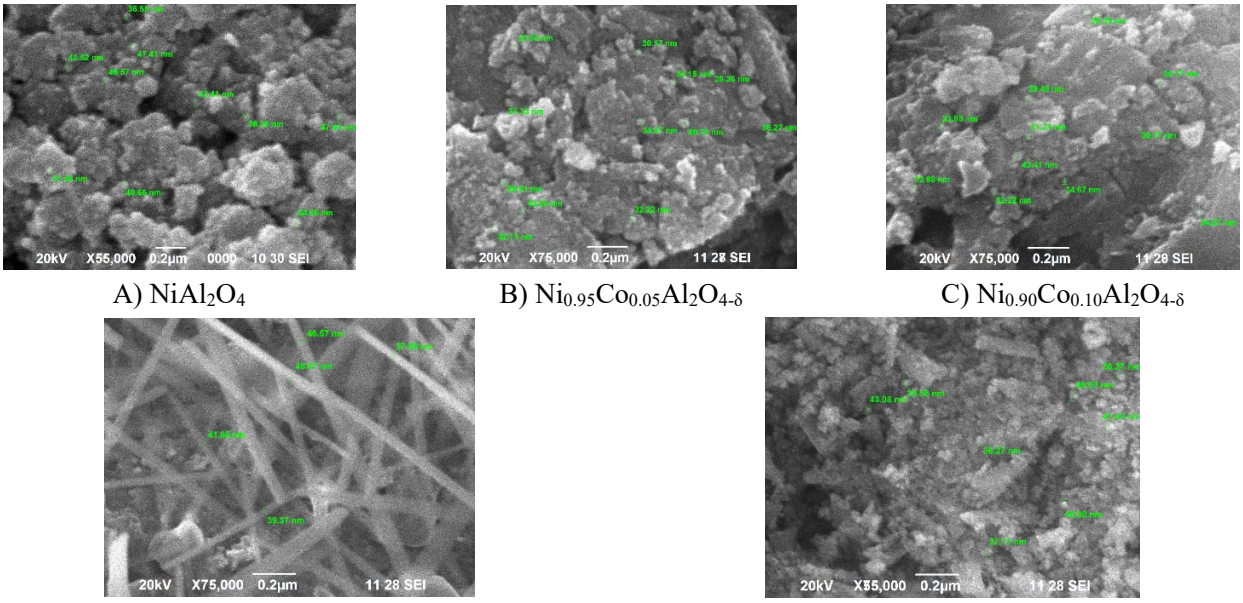

A) $NiAl_2O_4$ B) $Ni_{0.95}Co_{0.05}Al_2O_{4-\delta}$ C) $Ni_{0.90}Co_{0.10}Al_2O_{4-\delta}$

D) $Ni_{0.85}Co_{0.15}Al_2O_{4-\delta}$ E) $Ni_{0.80}Co_{0.20}Al_2O_{4-\delta}$

Fig. 6. SEM photographs obtained on $NiAl_2O_4$ based nanoparticles A) Parent $NiAl_2O_4$, B) $Ni_{0.95}Co_{0.05}Al_2O_{4-\delta}$, C) $Ni_{0.90}Co_{0.10}Al_2O_{4-\delta}$, D) $Ni_{0.85}Co_{0.15}Al_2O_{4-\delta}$, E) $Ni_{0.80}Co_{0.20}Al_2O_{4-\delta}$.

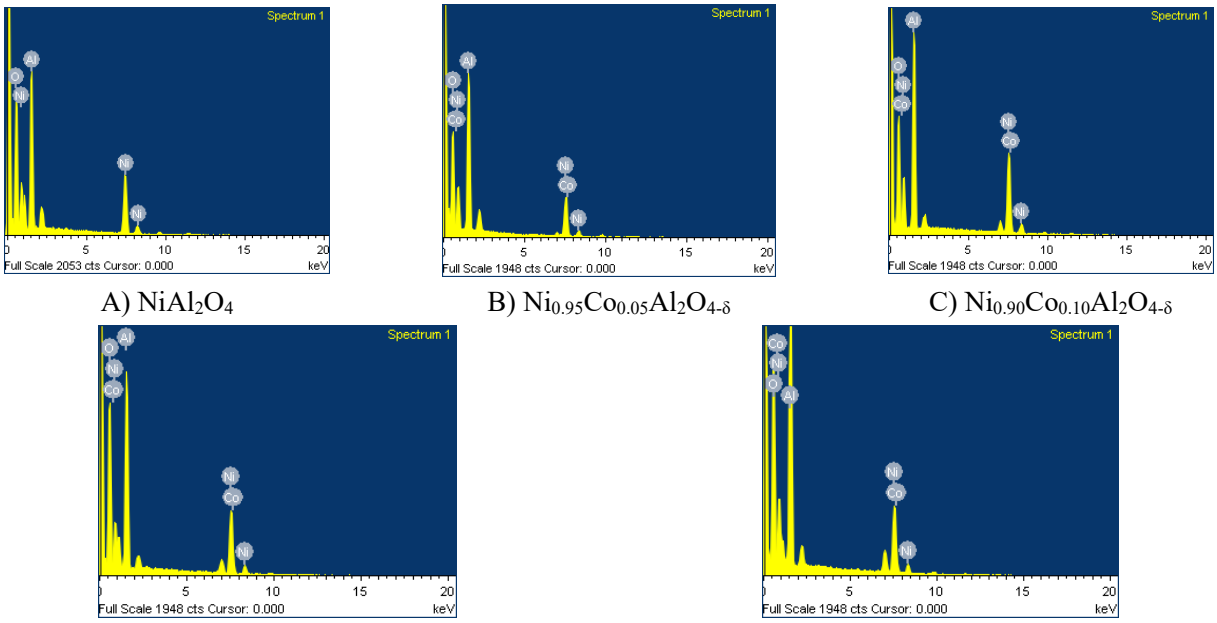

A) $NiAl_2O_4$ B) $Ni_{0.95}Co_{0.05}Al_2O_{4-\delta}$ C) $Ni_{0.90}Co_{0.10}Al_2O_{4-\delta}$

D) $Ni_{0.85}Co_{0.15}Al_2O_{4-\delta}$ E) $Ni_{0.80}Co_{0.20}Al_2O_{4-\delta}$

Fig. 7. EDX spectra obtained on $NiAl_2O_4$ based nanoparticles A) Parent $NiAl_2O_4$, B) $Ni_{0.95}Co_{0.05}Al_2O_{4-\delta}$, C) $Ni_{0.90}Co_{0.10}Al_2O_{4-\delta}$, D) $Ni_{0.85}Co_{0.15}Al_2O_{4-\delta}$, E) $Ni_{0.80}Co_{0.20}Al_2O_{4-\delta}$.

3.7. Studies on photoluminescence properties

The photoluminescence spectra (PL) of $NiAl_2O_4$ and Co doped $NiAl_2O_4$ nanoparticles is shown in Fig. 10. The PL spectra are observed at normal temperatures with a wavelength of 310 nm. This wavelength is finalized by the results of UV visible spectrum. From the PL spectra, it is found that the strong peaks were observed around 450 nm. According to the already existed PL data, the peaks present around 450nm attributed to the blue [45] emission of the visible region. Likewise, the existence of a strong peak is in accordance with the multilevel or multi-photon processes [46]. The concentration of the PL peak can be regulated by the amount of charge transferals and surface flaws, also the presence of some organic lasting (e.g., NO_3^-, CO_2) [47, 48].

Table 4. Elemental composition data obtained on $NiAl_2O_4$ and Co doped $NiAl_2O_4$ nanoparticles.

Sample	Nickel		Cobalt		Aluminium		Oxygen	
	Atomic %	Weight %	Atomic %	Weight %	Atomic %	Weight %	Atomic %	Weight %
$NiAl_2O_4$	10.82	25.22	0	0	24.91	31.07	64.27	43.71
$Ni_{0.95}Co_{0.05}Al_2O_{4-\delta}$	10.38	25.91	0.75	1.88	25.22	28.93	63.64	43.28
$Ni_{0.90}Co_{0.10}Al_2O_{4-\delta}$	11.84	30.01	1.4	3.11	25.91	26.54	60.85	40.34
$Ni_{0.85}Co_{0.15}Al_2O_{4-\delta}$	10.98	27.11	1.81	4.49	25.05	28.88	62.16	39.52
$Ni_{0.80}Co_{0.20}Al_2O_{4-\delta}$	10.02	23.52	2.37	5.94	24.04	27.59	63.58	42.95

3.8. Studies on photocatalytic degradation

The photocatalytic removal of malachite green (MG) was investigated by nanosized $NiAl_2O_4$ and Co doped $NiAl_2O_4$ catalysts. The chemical structure of malachite green (MG) dye is shown in Fig. 11. For each experiment, 50ml of the dye solution(0.2g/l of malachite green) is taken and the photocatalyst (5mg) is added into the dye solution. Then, the solution is mixed and agitated well for 60 minutes without light to attain equilibrium. After attaining equilibrium, the dye solution is transferred into a photoreactor equipped with visible light and the UV visible spectra at various time interims (0, 30, 60, 90 and 120 minutes) is taken and the results are indicated in Fig. 12. The UV spectra denote a typical peak maximum at 616 nm. As the light passing time increases, the concentration of the peak observed at 616 nm diminishes. This is because of the elimination of MG in the presence of nanophotocatalysts ($NiAl_2O_4$ and Co doped $NiAl_2O_4$) under visible irradiation. From the results, it was found that sample A (parent $NiAl_2O_4$) degraded around 42% whereas the Co doped $NiAl_2O_4$ degraded around 20-39% after 2 hours of exposure in visible light.

The degradation percentage is lower in the Co doped $NiAl_2O_4$ which may be either due to recombination or also due to the inappropriate electronic structure of the doped metal [49]. Hence, it was concluded that $NiAl_2O_4$ is more efficient compared to Co doped $NiAl_2O_4$ nanophotocatalysts. A graph plotted between ln C_t/C_0 against time is shown in Fig. 13. Photocatalytic degradation follows a pseudo first-order reaction mechanism provided by Langmuir-Hinshelwood [50] (Eq. 6).

$$\ln C_t/C_0 = - kt \quad \textbf{(6)}$$

where, 'C_0' is the initial strength of MG dye, 'C_t' is the strength of MG dye at time 't', 'k' is the rate constant. The slope of these lines gives the value of rate constant. The values of 'k' obtained is 0.010 min^{-1} (MG dye), 0.1793 min^{-1} ($NiAl_2O_4$), 0.1624 min^{-1} ($Ni_{0.95}Co_{0.05}Al_2O_{4-\delta}$), 0.058 min^{-1} ($Ni_{0.9}Co_{0.1}Al_2O_{4-\delta}$), 0.1707 min^{-1} ($Ni_{0.85}Co_{0.15}Al_2O_{4-\delta}$) and 0.068 min^{-1} ($Ni_{0.8}Co_{0.2}Al_2O_{4-\delta}$). From the results, it was discovered that the catalytic activity of parent $NiAl_2O_4$ photocatalysts is greater than all other compositions of Co doped $NiAl_2O_4$ photocatalysts.

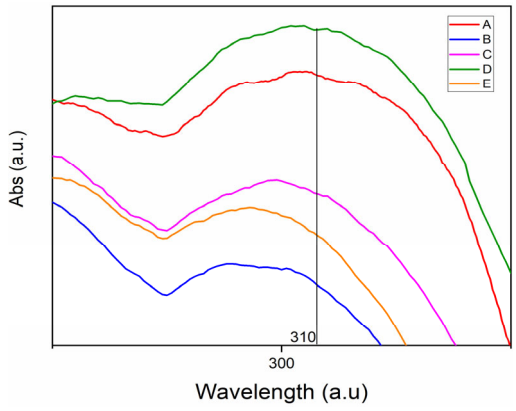

Fig. 8. UV visible spectrum obtained on $NiAl_2O_4$ based nanoparticles A) Parent $NiAl_2O_4$, B) $Ni_{0.95}Co_{0.05}Al_2O_{4-\delta}$, C) $Ni_{0.90}Co_{0.10}Al_2O_{4-\delta}$, D) $Ni_{0.85}Co_{0.15}Al_2O_{4-\delta}$, E) $Ni_{0.80}Co_{0.20}Al_2O_{4-\delta}$

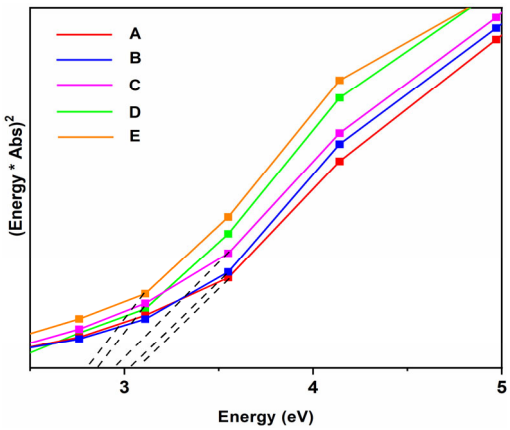

Fig. 9. Band gap spectrum obtained on $NiAl_2O_4$ based nanoparticles A) Parent $NiAl_2O_4$, B) $Ni_{0.95}Co_{0.05}Al_2O_{4-\delta}$, C) $Ni_{0.90}Co_{0.10}Al_2O_{4-\delta}$, D) $Ni_{0.85}Co_{0.15}Al_2O_{4-\delta}$, E) $Ni_{0.80}Co_{0.20}Al_2O_{4-\delta}$

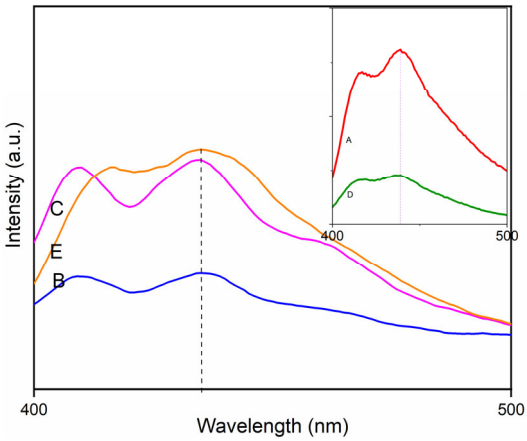

Fig. 10. The PL spectrum obtained on $NiAl_2O_4$ based nanoparticles A) Parent $NiAl_2O_4$, B) $Ni_{0.95}Co_{0.05}Al_2O_{4-\delta}$, C) $Ni_{0.90}Co_{0.10}Al_2O_{4-\delta}$, D) $Ni_{0.85}Co_{0.15}Al_2O_{4-\delta}$, E) $Ni_{0.80}Co_{0.20}Al_2O_{4-\delta}$.

When the $NiAl_2O_4$ and Co doped $NiAl_2O_4$ catalysts were irradiated by light, holes in the VB will be made as the electrons in the VB and they got energized and bounced to the CB. These opened holes are reacted with the encompassing H_2O and delivered profoundly receptive hydroxyl radicals ($OH^{\bullet}$). Also, the highly receptive oxygen radicals ($^{\bullet}O_2^-$) are formed when the generated electrons (e^-) react with the atmospheric oxygen molecules (O_2). These reactive species are the source for MG degradation [51-53] (Eqs. 7-11).

$$NiAl_2O_4 + h\nu \rightarrow NiAl_2O_4\ 2(e^- + h^+) \quad \textbf{(7)}$$

$$e^- + O_2 \rightarrow O_2^{\bullet -} \quad \textbf{(8)}$$

$$2e^- + O_2 + 2H^+ \rightarrow H_2O_2 \quad \textbf{(9)}$$

$$H_2O_2 + O_2^{\bullet -} \rightarrow OH^- + OH^{\bullet} \quad \textbf{(10)}$$

$$OH^{\bullet}/h^+ / {}^{\bullet}O_2^- + MG \rightarrow \text{Degraded product} \quad \textbf{(11)}$$

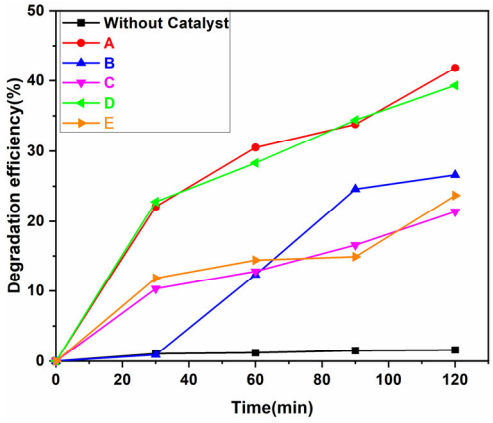

Fig. 12. Degradation spectrum of MG dye in the presence of A) Parent $NiAl_2O_4$, B) $Ni_{0.95}Co_{0.05}Al_2O_{4-\delta}$, C) $Ni_{0.90}Co_{0.10}Al_2O_{4-\delta}$, D) $Ni_{0.85}Co_{0.15}Al_2O_{4-\delta}$, E) $Ni_{0.80}Co_{0.20}Al_2O_{4-\delta}$.

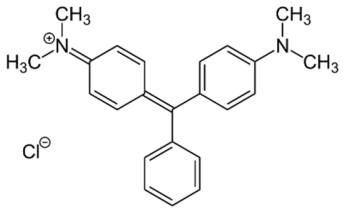

Fig. 11. Structure of malachite green (MG) dye.

4. Conclusions

The $NiAl_2O_4$ and Co doped $NiAl_2O_4$ nanoparticles were synthesized by the simple, low-temperature wet chemical synthesis route. The synthesized materials were confirmed by XRD, FTIR, particle size, SEM, EDX and UV and PL. XRD data confirmed the presence of a cubic (FCC) phase in all the samples. FTIR data confirmed bonds related to the tetrahedral and octahedral sites of the spinel. Particle size data indicated the presence of particles between 36-741 nm. The presence of nano and micron-sized grains in the samples was confirmed by SEM analysis. EDX data shows the occurrence of appropriate quantities of Ni, Al, Co, and O in the samples. The band gap of $NiAl_2O_4$ is found to be around 2.8 – 3.0 eV, which is in good agreement with the literature. The PL spectra exhibited a strong peak at around 450 nm in the samples. Among the samples studied, the parent $NiAl_2O_4$ shows more efficiency in degrading the malachite green (MG dye) than other Co doped $NiAl_2O_4$ photocatalysts under visible light irradiation at the wavelength of 616nm at normal temperature. This may be due to the recombination of the species or may be due to the electronic structure of the dopants. The obtained findings reveal that $NiAl_2O_4$ nanoparticle is a possible contender for the photocatalytic applications and can be used to eliminate very toxic dyes such as MG existed in aqueous medium by photocatalysis at normal temperature.

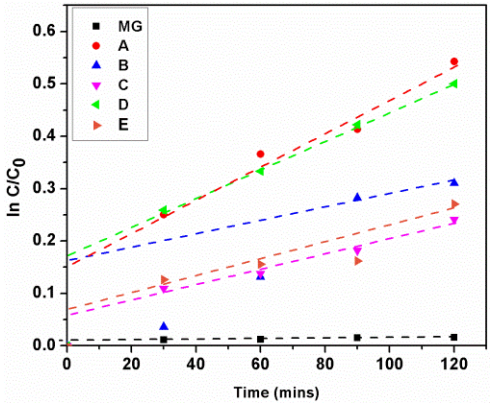

Fig. 13. First-order kinetic plot of MG dye using A) Parent $NiAl_2O_4$, B) $Ni_{0.95}Co_{0.05}Al_2O_{4-\delta}$, C) $Ni_{0.90}Co_{0.10}Al_2O_{4-\delta}$, D) $Ni_{0.85}Co_{0.15}Al_2O_{4-\delta}$, E) $Ni_{0.80}Co_{0.20}Al_2O_{4-\delta}$ and with no photocatalyst.

Acknowledgements

ASN thanks the Karunya Institute of Technology and Sciences (KITS) for promoting nanomaterials chemistry based research activity in the Department of Applied Chemistry. MAK thanks KITS for providing necessary research facilities to carry out this research work.

References

[1] M. Mohamed Jaffer Sadiq, A. Samson Nesaraj, J. Nanostruct. Chem. 5 (2015) 45–54.
[2] A. Ameta, R. Ameta, M. Ahuja, Sci. Revs. Chem. Commun. 3 (2013) 172–180.
[3] D. Mahanta, G. Madras, S. Radhakrishnan, S. Patil, J. Phys. Chem. B, 112 (2008) 10153-10157.
[4] Z. Mehrabadi, H. Faghihian, Spectrochim. Acta A 204 (2018) 248–259.
[5] K.T. Ranjit, B. Viswanathan, J. Photochem. Photobiol. A 108 (1997) 79-84.
[6] M. Abedi, G. Mahmoudi, P. Hayati, B. Machura, F. I. Zubkov, K. Mohammadi, S. Bahrami, H. Derikvandi, Z. Mehrabadih, A. M. Kirillov, New J. Chem. 43 (2019) 17457–17465.
[7] Z. Mehrabai, H. Faghihian, Mater. Res. Bull. 119 (2019) 110569.
[8] H. Derikvandi, A. Nezamzadeh-Ejhieh, Solid State Sci. 101 (2020) 106127.
[9] S. Ghattavi, A. Nezamzadeh-Ejhieh, Composites Part B 183 (2020) 107712.
[10] S. Jafari, A. Nezamzadeh-Ejhieh, J. Colloid Interface Sci. 490 (2017) 478–487.
[11] A. Khatri, M. Hussain Peerzada, M. Mohsin, M. White, J. Cleaner Prod. 87 (2015) 50-57.
[12] A. Buthiyappan, A. R. Abdul Aziz, W. M. A. Wan Daud, Rev. Chem. Eng. 32 (2016) 1-47.
[13] S. Benkhaya, S. M'rabet, A. El Harfi, Inorg. Chem. Commun. 115 (2020) 107891.
[14] A. Azari, R. Nabizadeh, S. Nasseri, A. H. Mahvi, A R. Mesdaghinia, Chemosphere 250 (2020) 126238.
[15] V. Katheresan, J. Kansedo, S. Y. Lau, J. Environ. Chem. Eng. 6 (2018) 4676–4697.
[16] A. Nezamzadeh-Ejhieh, H. Zabihi-Mobarakeh, J. Ind. Eng. Chem. 20 (2014) 1421–1431.
[17] A. Nezamzadeh-Ejhieh, Z. Banan, Desalination, 284 (2012) 157–166.
[18] N.M. Deraz, Int. J. Electrochem. Sci. 8 (2013) 5203–5212.
[19] C. Ragupathi, J. Judith Vijaya, P. Surendhar, L. John Kennedy, Polyhedron 72 (2014) 1-7.
[20] Z. Mehrabadi, H. Faghihian, J. Photochem. Photobiol. A 356 (2018) 102–111.
[21] H. Katayama-Yoshida, T. Nishimatsu, T. Yamamoto, N. Orita, J. Phys. Condens. Matter 13 (2001) 8901–8914.
[22] M. Maddahfar, M. Ramezani, M.Sadeghi, A. Sobhani-Nasab, J. Mater. Sci. Mater. Electron. 26 (2015) 7745–7750.
[23] H. Zhao, L. Liu, B. Wang, D. Xu, L. Jiang, C. Zheng, Energy Fuels 22 (2008) 898-905.
[24] P. Jeevanandam, Y. Koltypin, A. Gedanken, Mater. Sci. Eng. B 90 (2002) 125-132.
[25] S.G. Menon, H.C. Swart, J. Alloys Compd. 819 (2020) 152991.
[26] C. Ragupathi, J. Judith Vijaya, L. John Kennedy, J. Saudi Chem. Soc. 21 (2017) S231-S239.
[27] J. W. Kim, P.W. Shin, M. J. Lee, S. J. Lee, J. Ceram. Process. Res. 7 (2006) 117–121.
[28] Y. Cesteros, P. Salagre, F. Medina, J.E. Sueiras, Chem. Mater. 12 (2000) 331–335.
[29] Z. Boukha, C. Jimenez-Gonzalez, B. de Rivas, J.R. Gonzalez-Velasco, J. I. Gutierrez-Ortiz, R. Lopez-Fonseca, Appl. Catal. B 158-159 (2014) 190-201.
[30] C. Jiménez-González, Z. Boukha, B. de Rivas, J.R. González-Velasco, J. I. Gutiérrez-Ortiz, R. López-Fonseca, Energy Fuels 28 (2014) 7109–7121.
[31] N. A. Dahoudi, Q. Zhang, G. Cao, Int. J. Photoenergy 2012 (2012) 401393.
[32] Y. Huan, G. Wang, C. Li, G. Li, J. Mater. Sci. 55 (2020) 4656–4670.
[33] F. Zakika, M. Benamira, H. Lahmar, A. Tibera, R.Chabi, I. Avramova, S. Suzer, M.Trari, J. Photochem. Photobiol. A 364 (2018) 542–550.
[34] T. Tangcharoen, J. T-Thienprasert, C. Kongmark, J. Mater. Sci. Mater. Electron. 29 (2018) 8995–9006.
[35] I.A. Amar, H. M. Harara, Q. A. Baqul, M.A.A. Qadir, F. A. Altohami, M.M. Ahwidi, I. A. Abdalsamed, F.A. Saleh, Asian J. Nanosci. Mater. 3 (2020) 1-14.
[36] R. M. Mohamed, E. S. Baeissa, I. A. Mkhalid, M.A. Al-Rayyani, App. Nanosci. 3 (2013) 57-63.
[37] M. Balakrishnan, R. John, Iran. J. Catal. 10 (2020) 1–16.
[38] C.N.R. Rao, Chemical applications of infrared spectroscopy, Academic Press, New York, 1963.
[39] K.D. Lee, J. Korean Phys. Soc. 38 (2001) 33-37.
[40] F. Ahangaran, A. Hassanzadeh, S. Nouri, Int. Nano Lett. 3 (2013) 23.
[41] R. Tiwari, M. De, H. S. Tewari, S. K. Ghoshal, Results Phys. 16 (2020) 102916.
[42] L.Truffault, M. Ta, T. Devers, K. K. Konstantinov, V. Harel, C. Simmonard, C. Andreazza, I. Nevirkovets, A. Pineau, O. Veron, J. Blondeau, Mater. Res. Bull. 45 (2010) 527-535.
[43] A. Cimino, M. Lo Jacono, M. Schiavello, J. Phys. Chem. 75 (1971) 1044–1050.
[44] J. Karpińska, U. Kotowska, Water 11(2019) 2017.
[45] L. S. Cavalcante, J. C. Sczancoski, L. F. Lima, Jr., J. W. M. Espinosa, P. S. Pizani, J. A. Varela, E. Longo, Cryst. Growth Des. 9 (2009) 1002–1012.
[46] Y. Yin, Z. Gan, Y. Sun, B. Zhou, X. Zhang, D. Zhang, P. Gao, Mater. Lett. 64 (2010) 789–792.
[47] C. Ragupathi, J. J.Vijaya, S. Narayanan, L. John Kennedy, S. Ramakrishna, Chin. J. Catal. 34 (2013) 1951–1958.
[48] S.-F.Wang, G.-Z. Sun, L.M. Fang, L. Lei, X. Xiang, X.-T. Zu, Sci. Rep. 5 (2015) 12849.

[49] A. Dhakshinamoorthy, M. Alvaro, H. Garcia, Catal. Sci. Technol. 1 (2011) 856–867.
[50] S. Pan, X. Liu, New. J. Chem. 36 (2012) 1781-1787.
[51] R.K. Mandal, M.D. Purkayastha, T.P. Majumder, Optik 180 (2019) 174-182.
[52] L. Saikia, D. Bhuyan, M. Saikia, B. Malakar, D. K. Dutta, P. Sengupta, Appl. Catal. A 490 (2015) 42-49.
[53] R. Murugan, L. Kashinath, R. Subash, P. Sakthivel, K. Byrappa, S. Rajendran, G. Ravi, Mater. Res. Bull. 97 (2018) 319-325.